Ice loss in High Mountain Asia and the Gulf of Alaska observed by CryoSat-2 swath altimetry between 2010 and 2019

Livia Jakob[1], Noel Gourmelen[1,2,3], Martin Ewart[1], Stephen Plummer[4]

[1]Earthwave Ltd, Edinburgh, EH9 3HJ, United Kingdom
5   [2]School of GeoSciences, University of Edinburgh, Edinburgh, EH8 9XP, United Kingdom
[3]IPGS UMR 7516, Université de Strasbourg, CNRS, Strasbourg, F-67000, France
[4]European Space Agency, ESA-ESTEC, Noordwijk, 2201 AZ, Netherlands

Correspondence to: Livia Jakob (livia@earthwave.co.uk)

Abstract. Glaciers and ice caps are currently the largest non-steric contributor to sea level rise, contributing ~30% to sea level
10   budget. Global monitoring of these regions remains a challenging task since global estimates rely on a variety of observations
and models to achieve the required spatial and temporal coverage, and significant differences remain between current
estimates. Here we report the first application of a novel approach to retrieve spatially-resolved elevation and mass change
from Radar Altimetry over entire mountain glaciers areas. We apply interferometric swath altimetry to CryoSat-2 data acquired
between 2010 and 2019 over High Mountain Asia (HMA) and in the Gulf of Alaska (GoA). In addition, we extract monthly
15   time series of elevation change, exploiting CryoSat's high temporal repeat, to reveal seasonal and multiannual variation in
rates of glaciers' thinning at unprecedented spatial detail. We find that during this period, HMA and GoA have lost an average
of -27.9 ± 2.4 Gt yr^{-1} (-0.29 ± 0.03 m w.e. yr^{-1}) and -76.3 ± 5.6 Gt yr^{-1} (-0.89 ± 0.07 m w.e. yr^{-1}) respectively, corresponding
to a contribution to sea level rise of 0.048 ± 0.004 mm yr^{-1} and 0.217 ± 0.015 mm yr^{-1}. Glacier thinning is ubiquitous except
for the Karakoram-Kunlun region experiencing stable or slightly positive mass balance. In the GoA region, the intensity of
20   thinning varies spatially and temporally and correlates with the strength of the Pacific Decadal Oscillation. In HMA we observe
sustained multiannual trends until 2015-6, and decreased loss or even mass gain from 2016-17 onwards.

1   Introduction

Mountain glaciers store less than 1% of the global ice mass (Farinotti et al., 2019) however their rapid rate of mass loss
accounts for almost a third of the global sea level rise, the largest sea level rise (SLR) contribution from land-ice (Gardner et
25   al., 2013; Shepherd et al., 2020; Zemp et al., 2019). Besides representing an icon for climate change (Bojinski et al., 2014) and
impacting global sea level rise, the retreat and thinning of mountain glaciers also affects local communities (Immerzeel et al.,
2010). Glacier retreat introduces substantial changes in seasonal water availability, which can have major societal impacts
downstream, such as endangering water security for populations relying on surface water, or introducing extreme flooding
(Guido et al., 2016; Ragettli et al., 2016).

30   The quantification of mass loss in mountain glaciers has posed scientific challenges, resulting in the need to combine various types of observation, and the need to reconcile results obtained using different methods (Gardner et al., 2013). The traditional approach (glaciological method) extrapolates in situ observations (Bolch et al., 2012; Cogley, 2011; Yao et al., 2012; Zemp et al., 2019), however measurements are sparse and possibly biased towards better accessible glaciers located at lower altitudes (Fujita and Nuimura, 2011; Gardner et al., 2013; Wagnon et al., 2013). More recent geodetic remote sensing methods include

35   (1) Digital Elevation Model (DEM) differencing (Berthier et al., 2010; Brun et al., 2017; Gardelle et al., 2013; Maurer et al., 2019; Shean et al., 2020), (2) satellite laser altimetry (Kääb et al., 2012, 2015; Neckel et al., 2014; Treichler et al., 2019) and (3) Gravity Recovery and Climate experiment (GRACE) satellite gravimetry (Ciracì et al., 2020; Gardner et al., 2013; Jacob et al., 2012; Luthcke et al., 2008; Wouters et al., 2019).

Despite substantial advances with geodetic remote sensing methods, enhancing the spatial resolution and coverage of ice loss

40   estimates (e.g. Brun et al., 2017), there is currently no demonstrated operational system that can routinely and consistently monitor glaciers worldwide, especially in rugged mountainous terrain and with the necessary temporal resolution. Seasonal changes in surface elevation change are key to improving our understanding of the climatic processes that drive surface mass balance in mountain glaciers. Moreover, seasonal melt cycles of mountain glaciers have downstream impacts on livelihoods exposed to glacial risk, such as geohazards (glacier lake outbursts, glacier lake expansion, flooding) and water and food security

45   (Huss and Hock, 2018; Pritchard, 2019).

Prior to CryoSat-2, radar altimetry has traditionally been limited to regions of moderate topography such as ice sheets. The launch of a dedicated radar altimetry ice mission, CryoSat-2, improvement in the ability to accurately map the ground position of the radar echoes, and the full use of the returned waveform via swath processing (Gourmelen et al., 2018; Gray et al., 2013; Hawley et al., 2009), has seen a near-global expansion of its application to monitoring ice mass changes beyond the two large

50   ice sheets (Foresta et al., 2016; Gourmelen et al., 2018; Gray et al., 2015; McMillan et al., 2014b). Over regions of more extreme surface topography however, such as those found in mountain glacier areas, the use of radar altimetry has been prohibited by the large pulse-limited footprint. While CryoSat's sharper footprint has led to a few promising studies over mountain glaciers (Dehecq et al., 2013; Foresta et al., 2018; Trantow and Herzfeld, 2016), there remain two limiting factors for all radar altimeters for these elevation ranges, the limited range window (240 m for CryoSat) and the closed-loop onboard

55   tracking used to position the altimeter's range window; these 2 factors lead to a decrease in usable data in these environments (Dehecq et al., 2013).

The emphasis in this study is to demonstrate the ability of interferometric radar altimetry to monitor regional mass changes in challenging rugged terrain, despite the abovementioned limitations. For this demonstration, we chose High Mountain Asia (HMA) and the Gulf of Alaska (GoA), two regions with complex terrain which have not been previously monitored with radar

60   altimetry. We use CryoSat-2 swath altimetry to derive elevation and mass changes of mountain glaciers from 2010 to 2019, in addition, we exploit the repeat cycle of CryoSat-2 to generate time series (30 days steps) at sub-regional level, giving new insights into seasonal and interannual changes within the two regions. With this study, we ultimately aim to demonstrate the

potential of interferometric radar systems to contribute an independent observation of ice trends on a global scale and at high temporal resolution.

65

The HMA study area includes the Himalayan Mountain Range, the Tibetan Plateau and the Tien Shan mountains (regions 13, 14 and 15 of the Randolph Glacier Inventory) and is covered by about 100,000 km^2 of glacier area for a total of 95,540 glaciers (RGI Consortium, 2017). Climatic conditions in HMA are characterised by two main atmospheric circulation systems which impact the distribution of glaciers and glaciological changes; the Westerlies and the Indian monsoon (Figure 1). The Westerlies

70 dominate regions in the northwest (Pamir regions, Kunlun Shan, Tien Shan and western Himalayan mountain range) and are responsible for a large fraction of the precipitation deposited particularly during the winter months (Bolch et al., 2012; Li et al., 2015; Yao et al., 2012). The Indian summer monsoon mainly influences glaciers in southern sub-regions (central and eastern Himalayan mountains, Karakoram, Nyainqêntanglha mountains), with decreasing precipitation northward (Bolch et al., 2012; Yao et al., 2012). In contrast to the monsoonal and westerly regimes, the inner Tibetan Plateau is mainly dominated

75 by dry continental climatic conditions. Various studies have found precipitation increases in the Pamir regions and decreases in the central/eastern Himalayan range, affected by changes in the two atmospheric systems, namely the strengthened Westerlies and the weakening Indian Monsoon (Treichler et al., 2019; Yao et al., 2012). As a result of atmospheric forcing, the vast majority of glaciers in the HMA region have been losing mass since the beginning of the satellite records (Bolch et al., 2019; Maurer et al., 2019) which has led to widespread glacier slowdown (Dehecq et al., 2019).

80

The GoA region, which we define to encompass the mountain range stretching along the Gulf of Alaska to British Columbia (Region 1 of the Randolph Glacier Inventory 6.0, excluding Northern Alaska) is covered by approximately 86,000 km^2 glacier area for a total of 26,490 glaciers (RGI Consortium, 2017). The glacierised areas stretch from sea level up to over 5000 m. a.s.l., representing a large variety of different glacier types. 67% of the glacier area are in land-terminating glaciers, 13% and

85 20% are marine-terminating and lake-terminating respectively (Figure 1). Large glacier-to-glacier variations in mass changes have been reported, which are assumed to be driven by climate variability and heterogeneity of glacier elevation ranges (Larsen et al., 2015). The coastal regions along the Alaskan Gulf experience a maritime climate, with the maximum precipitation occurring on the southern slopes of the Coastal Range (Wendler et al., 2017). These mountain ranges act as barriers for the moist air from the Pacific Ocean resulting in rain shadow, i.e. more continental climate, on their leeward side (Le Bris et al.,

90 2011; Wendler et al., 2017). The Pacific Decadal Oscillation (PDO) is another factor which exercises substantial influence on the climate (Wendler et al., 2017) and glacier behaviour (Hodgkins, 2009) within the GoA region. In general, the positive phase of the PDO relates to higher temperatures and more precipitation (Fleming and Whitfield, 2010), whilst a cooling and decrease of precipitation are observed during its negative phase (Papineau, 2001). However, the effects on precipitation especially are spatially heterogenous (Fleming and Whitfield, 2010). Our study period of 2010 to 2019 contains the 2014

95 change from a negative phase of the PDO to a positive phase, contributing to a substantial increase in temperatures in Alaska from 2014 onwards (Wendler et al., 2017). As a result of atmospheric and oceanic forcings, glaciers in the GoA region have

been losing mass since the beginning of the satellite records (Arendt et al., 2002; Berthier et al., 2010; Wouters et al., 2019; Zemp et al., 2019).

2   Data and Methods

100   In this section, we give a short overview on the data and methods used in this study. More details can be found in the Supporting Information.

2.1   Time-dependent elevation from CryoSat-2 observations

We use observations from the SAR Interferometric Radar Altimeter (SIRAL) onboard the European Space Agency (ESA) CryoSat-2 satellite (Wingham et al., 2006). SIRAL is a beam-forming active microwave radar altimeter with a maximum
105   imaging range of ~15 km on the ground. The sensor emits time-limited *Ku-band* pulses aimed at reducing the footprint to ~1.6 km within the beam. Over land-ice, the sensor operates in synthetic aperture interferometric (SARIn) mode, which allows delay-Doppler processing to increase the along-track resolution to ~380 m, while cross-track interferometry is used to extract key information about the position of the footprint centre. CryoSat-2 orbits the Earth with a 369-day near-repeat period formed by the successive shift of a 30-day sub-cycle. The satellite has an inclination of 92°, offering improved coverage of the polar
110   regions. We process *level 1b,* baseline C data and the corrected mispointing angle for aberration of light (Scagliola et al., 2018) supplied by the ESA ground segment using a swath processing algorithm (Gourmelen et al., 2018). *Level 1b* data is provided as a sequence of radar echoes along the satellite track, which translates into single power, interferometric phase and coherence waveforms for each along-track location. The conventional *level 1b* data processing method consists in extracting single elevation measurements from the power signal in each waveform that corresponds to the Point of Closest Approach (POCA)
115   between satellite and the ground. In contrast, swath altimetry exploits the full radar waveform to map a dense swath (~5 km wide) of elevation measurements across the satellite ground track beyond POCA (Foresta et al., 2016, 2018; Gourmelen et al., 2018; Gray et al., 2013; Hawley et al., 2009) providing one to two orders of magnitude more elevation measurements compared with POCA. This makes the CryoSat-2 sensor at present the only radar altimeter able to survey small glaciers and ice caps at high resolution.

120   ### 2.2   Rates of elevation change maps

Rates of elevation change and mass balance are based on ~25 million swath elevation measurements in the GoA region and ~8 million swath elevation measurements in HMA from 2010 to 2019. The altitudinal distribution of the measurements departs somewhat from the glaciers' hypsometry. Given the general correlation between ice thickness change and hypsometry in the region of imbalance, a bias in the altitudinal distribution of observations can lead to a bias in the total rate of thinning when
125   integrated over a larger domain. Therefore we derive a subset of the time-dependent elevation dataset, removing the impact of such point density biases by filtering out swath measurements so as to match the glacier hypsometry (e.g. Treichler et al.,

2019), and generate elevation change and mass change estimates from the reduced sample (Figure S4). We remove data sequentially based on measurement uncertainty. This process reduces our sample size by 15% for the GoA and by 30% for HMA. To generate rates of elevation change we then follow a similar approach to Foresta et al. (2016) and Gourmelen et al.

130 (2018), however the lower data density and the complexity of the terrain in the GoA region and in HMA require a slight adaptation of the methodology. We bin the elevation measurements into regions of 100 x 100 km, sufficiently large to contain the necessary number of measurements in each bin to ensure sufficient robustness and representativity. Due to the increased bin size (the pixel size used by Foresta et al. [2016] and Gourmelen et al. [2018] is 1000 m) and the variation of elevations within each bin, the topographic signature cannot simply be modelled and therefore needs to be removed using an auxiliary

135 Digital Elevation Model (DEM) (Kääb et al. 2012). We subtract the TanDEM-X 90m DEM (German Aerospace Center [DLR], 2018), which has a near-complete coverage and is contemporaneous of the CryoSat-2 observations, from the swath elevation measurements. The remaining elevation differences (hereinafter referred to as *elevDiff*) are due to time-dependent elevation change that can be related to glacier thickness change as well as errors in the two data sets, temporal heterogeneity and differences in penetration between the reference DEM and the swath elevation measurements.

140 Time-dependent rates of surface elevation change are calculated for each 100 x 100 km bin individually based on the *elevDiff* measurements. In order to achieve the most robust trends we considered several fitting methods, including ordinary least-square, robust regression (e.g. Kääb et al., 2012, 2015), weighted regression (e.g. Berthier et al., 2016; Foresta et al., 2018; Gourmelen et al., 2018), random sample consensus (RANSAC) and Theil-Sen estimator (e.g. Shean et al., 2020). We found that the best results were achieved with a weighted regression model of the *elevDiff* measurements, similar to the methods of

145 Gourmelen et al. (2018). However, whilst their weights are calculated only according to the power attribute, here we assign each observation a weight based on power and coherence, i.e. measurements with high power and low coherence within the sample will have lower weights assigned (see Supplementary Information S1.1). When fitting the model, we iteratively exclude measurements that are more than 3σ from the mean distance to the fitted line, until no more outliers are present (e.g. Foresta et al., 2016, 2018). The rate of change uncertainty is extracted from the standard error of the regression model. We

150 conservatively use a factor of five for uncertainties on areas without coverage of swath measurements (see Supplementary Information S1.4). After generating time-dependent elevation changes and elevation change uncertainty for each 100 x 100 km bin we discarded bins that did not fulfil a set of quality criteria (see Supplementary Information S1.2). The remaining bins covered more than 96% of the total glacierised area in the GoA region, and ~90% in HMA. To estimate values for the gaps in our dh/dt map we use the altitudinal distribution of elevation change rates on a sub-regional level (Moholdt et al., 2010a,

155 2010b; Nilsson et al., 2015), applying the hypsometric averaging methods described in the Supplementary Information (S1.3). It is a well known observation that microwave pulses scatter from the surface as well as the subsurface, which can lead to elevation change bias in regions of historically anomalous melt event (Nilsson et al., 2015); over most regions however, it has been shown that surface elevation change from CryoSat is consistent with in-situ, airborne, and meteorological observations (Gourmelen et al., 2018; Gray et al., 2015; McMillan et al., 2014a; Zheng et al., 2018)

2.3 Mass balance and contribution to sea level rise

To obtain volume changes we use the glacierised area of the Randolph Glacier Inventory (RGI 6.0) (RGI Consortium, 2017). We assume the standard bulk density of 850 kg/m^3 (Huss, 2013) to convert volume changes to equivalent mass changes. Mass change uncertainty is calculated based on the main three error sources: rates of change uncertainty, uncertainty of the glacierised area and volume-mass conversion uncertainty (see Supplementary Information S1.4). To obtain a region-wide mass balance, mass changes of each individual bin are summed up. We derive mass balance for the unadjusted (biased) and glacier hypsometry adjusted (unbiased) elevation dataset (see Section 2.2), our final mass balance numbers are for the unbiased case. To generate the contribution to sea level rise (SLR) we exclude large endorheic basins in High Mountain Asia and assume an area of the ocean of $361.8 \cdot 10^6$ km^2.

2.4 Time series of seasonal surface elevation changes

CryoSat-2's monthly repeat cycle provides the opportunity to monitor seasonal as well and multiannual trends of surface elevation. We therefore generate time series with a monthly step (30 days) and a 3-month (90 days) moving window, using the median of all the *elevDiff* observations (residuals from the reference DEM) within a time period with reference to the first month. Time series are generated on bin size level (100 x 100 km), on sub-regional level (using the RGI sub-regions) and for the full study region. The time series of the 100 x 100 km bins are mainly used as an additional check of the dh/dt quality (see Supplementary Information S1.2), whilst we exploit the sub-regional and regional time series to analyse spatio-temporal variability in thickness change across both, the GoA and HMA regions. To generate region-wide time series for HMA and the GoA we use an area-weighted mean of the sub-regional time series. Note that the regional and sub-regional time series displayed in this publication start in January 2011 (with the earliest data from November 2010 using the 90 days window), since we retrieve less swath measurements for the first few months of CryoSat-2's life cycle, impacting the quality of the time series pre-2011.

3 Results

3.1 Spatial coverage and elevation sampling

Using the pulse-limited footprint size of CryoSat-2, we achieve a total spatial coverage of glaciated regions of 55% in the GoA and 32% in HMA respectively. These values are the combined result of the absence of recorded returns due to orbit separation and onboard-tracking limitation (Dehecq et al., 2013), and of data quality. Given that 40% of HMA glaciers are not measured due to onboard tracking limitations (Dehecq et al., 2013) the rate coverage of the measurable area is about 50%. These values are within the high-end of the range of observational methods (Zemp et al., 2019), whist generally lower than the coverage provided by very-high resolution sensors (Brun et al., 2017; Shean et al., 2020). Despite the relatively large size footprint of

radar altimeters, we observe a coverage of all glacier sizes, with approximately 10% area of very small glaciers covered (Figure
190 S5), as expected we do observe a positive correlation between spatial coverage and glacier size.

Representative elevation sampling of swath measurements is important, since change in thickness is strongly correlated with elevation and any systematic elevation bias of the sampling has the potential to affect *dh/dt* trends. Spatial coverage and number of points show a different relationship with hypsometry, which is due to the overlap between adjacent CryoSat footprints. Comparing the glacier hypsometry with the spatial coverage of our data shows no significant region-wide elevation bias,
195 however, we observe a bias of the total number of swath measurements towards higher altitudes (e.g. Figure S4), which can be attributed to the onboard tracking tending to favour elevations closest to the satellite.

As expected, we retrieve slightly smaller specific mass losses with differences in the order of 0.05 m w.e. yr^{-1} for the GoA region and 0.02 m w.e. yr^{-1} for HMA without removing the elevation bias towards higher altitudes. We do not observe any significant changes in the overall spatial pattern of elevation change across the two regions between the unbiased and biased
200 results, which indicates that we still achieve a stable result with the reduced sample.

3.2   Elevation changes and mass balance in High Mountain Asia

The total unbiased HMA mass balance between 2010 and 2019 was –27.9 ± 2.4 Gt yr^{-1} (–0.29 ± 0.03 m w.e. yr^{-1}) and –18.3 ± 1.6 Gt yr^{-1} (–0.38 +- 0.03 m w.e. yr^{-1}) excluding endorheic basins. Our maps of surface elevation change show a heterogenous pattern in the Himalayan range, with a cluster of slightly positive/near balance trends in the Kunlun and Karakoram ranges
205 (Figure 2). This spatial pattern confirms the suggestion of previous studies (Brun et al., 2017; Gardner et al., 2013; Kääb et al., 2015), that the so-called "Karakoram anomaly" (Gardelle et al., 2012; Yao et al., 2012) stretches up to West Kunlun Shan, which has now become the centre of the anomaly. Another striking feature is the gradient from moderate thinning in Spiti-Lahaul and western Himalaya to increasingly negative surface elevation changes along the central and eastern Himalayan mountain range, with the Nyainqêntanglha mountains and Hengduan Shan showing the highest negative trends. In contrast
210 with other studies (Brun et al., 2017; Shean et al., 2020) we find a heterogenous pattern in the Tibetan Plateau and Eastern Kunlun, with some scattered glaciers displaying higher mass losses.

3.3   Glacier elevation changes and mass balance in the Gulf of Alaska

In general we find much higher mass losses in the Gulf of Alaska than in High Mountain Asia, in agreement with global studies (Gardner et al., 2013; Zemp et al., 2019). Over an area of ~86,000 km^2, including all 26,490 glaciers in the RGI region 1 except
215 Northern Alaska, we estimate a total mass balance of –76.3 ± 5.6 Gt yr^{-1} (–0.89 ± 0.07 m w.e. yr^{-1}), contributing –0.199 ± 0.015 mm yr^{-1} to global sea level rise. Surface elevation change maps (Figure 3) display an expected pattern with clearly visible higher negative trends towards lower elevations close to the coast. The largest mass loss is seen in the Coast Mountains and Saint Elias Mountains, especially the Yukutat and Glacier Bay region, which is in line with the spatial patterns of Luthcke et al. (2008) and Luthcke et al. (2013). The lowest thinning rates are observed in the Alaska Range mountains, which is also
220 in agreement with other studies (Berthier et al., 2010; Luthcke et al., 2008).

4 Discussion

4.1 High Mountain Asia

4.1.1 Temporal variability

We display temporal variability of surface elevation change for the whole HMA region (Figure 4), the RGI second order
225 regions (Figure 5, S1) and the regions by Brun et al. (2017) (Figure S2). The monthly time series show sustained multiannual
trends across almost all of the subregions until 2015-6, and decreased loss or even mass gain from 2016/2017 onwards (Figure
5, S2), which is also reflected in the full HMA time series (Figure 4). The Karakoram region in particular displays thinning
from 2011 to 2014/5 before abating and thickening again from 2016/7. This shift of thinning rates post-2015 is also clearly
seen in Bhutan/East Himalaya, Kunlun (West and East), Tien Shan, Pamir Alay/Hissar Alay and Nyainqêntanglha/Hengduan
230 Shan (Figure 5, S1, S2). The seasonal time series variability reveals the influence of weather patterns and atmospheric
circulations in High Mountain Asia on ice thickness change. Sub-regions dominated by the winter Westerlies, such as Tien
Shan, Hindu Kush, Western Himalaya and the Pamir region (see Pohl et al., 2015; Yao et al., 2012), show the typical seasonal
pattern with mass accumulation during winter/spring periods and mass losses in the summer/autumn months (Figure 5).
Contrarily, sub-regions influenced by the summer Indian monsoon (Central Himalaya, Eastern Himalaya and Hengduan Shan),
235 where glacier accumulation and ablation happen at the same time, show a more heterogenous seasonal pattern. In the time
series of these three subregions the annual cycle has two peaks, with the first peak reflecting thickening in winter and the
second and smaller peak reflecting the summer accumulation through the influence of the Indian summer monsoon (see Figure
S1). The inner Tibetan Plateau, dominated by a more continental climate, displays almost no intra-annual cycle. In general,
the heterogeneity of the time series reflects the sensitivity of mountain glaciers to meteorological patterns and changes.

240 #### 4.1.2 Altitudinal distribution

We display the altitudinal distribution of elevation changes in Figure 6 and a comparison with Brun et al. (2017) in Figure S6.
In general, we observe decreasing negative trends with increasing altitudes, which is an expected pattern (Brun et al., 2017;
Gardelle et al., 2013). We find the steepest gradient (Figure 6, S6, Table S3) in the Nyainqêntanglha/Hengduan Shan, which
is in line with the findings of Brun et al. (2017). We also observe lower or even inverse gradients in Bhutan/East Himalaya,
245 Spiti-Lahaul/West Himalaya, Karakoram/West-Kunlun and Pamir (Figure 6, S6, Table S3), which have been reported
previously and been related to debris thickness (Bisset et al., 2020; Brun et al., 2017). The main differences are observed in
the elevation profile of the Kunlun regions, where Brun et al. (2017) find constant thickening at all elevation during the survey
time period of 2000 to 2016, whilst we record thinning at lower elevations (see Figure 6). These findings suggest a shift towards
negative mass balance for the Kunlun region in comparison to the previous decade.

4.1.3 Comparison of regional mass balance with previous work

A comparison of mass balance results in the literature indicates that, while all the studies agree on the general trend in mass loss and spatial variability of mass loss, there is large degree of variability between estimates. While some of the variability can be attributed to the diversity of time-span and region boundaries used, there are also clear differences between observation methods (Figure 8a). Note that here we are only comparing region-wide mass trends with the results closest in space and time to this study, whilst sub-regional differences are discussed in the next section.

Our total mass balance of –27.9 ± 2.4 Gt yr⁻¹ (–0.29 ± 0.03 m w.e. yr⁻¹) is in good agreement with the –28.8 ± 12 Gt yr⁻¹ by Ciracì et al. (2020), a study based on the GRACE and GRACE Follow-On mission covering the period of 2002 to 2019. The results are similar to the estimates provided by various ICESat studies for the years 2003 to 2008, including the –28.8 ± 2.2 Gt yr⁻¹ by Treichler et al. (2019), the –24 ± 2 Gt yr⁻¹ by Kääb et al. (2015) (excludes the Tien Shan and the Inner Tibetan Plateau) and the –26 ± 12 Gt yr⁻¹ by Gardner et al. (2013) [based on ICESat and GRACE]. Our estimates are higher than recent DEM differencing studies such as the –19.0 ± 2.5 Gt yr⁻¹ (–0.19 ± 0.03 m w.e. yr⁻¹) by Shean et al. (2020) and the –16.3 ± 3.5 Gt yr⁻¹ (–0.16 ± 0.08 m w.e. yr⁻¹) by Brun et al. (2017).

Besides the differences in data and methodology, a part of these disagreements can be explained by the time periods. Maurer et al. (2019) find that the thinning rates in the Himalayas have almost doubled from the interval 1975–2000 to 2000–2016. This trend seems to have continued in more recent years, with Ciracì et al. (2020) observing an acceleration in mass loss of 10 ± 5 Gt yr⁻¹ per decade for the period of 2002 to 2019, which could explain our more negative mass balance in comparison to Brun et al. (2017) [2000 to 2016] and Shean et al. (2020) [2000 to 2018].

4.1.4 Comparison of sub-regional mass balances with previous work

Our higher regional mass loss when comparing to the two DEM differencing studies by Brun et al. (2017) and Shean et al. (2020) are mostly down to differences in the South-eastern Himalaya – especially Nyainqêntanglha/Hengduan Shan – and in the Pamir regions. We used the regions by Brun et al. (2017) and the RGI 6.0 second order regions to compare our results with other estimates (Figure 7, Figure S7, Table S1). For a full discussion of regional differences between estimates of recent studies refer to Bolch et al. (2019). Our results are in line with general findings by Bolch et al., (2019) in the sense that we obtain similar results in sub-regions where there is a good agreement in general between studies, such as Tien Shan, Karakoram, West Nepal (West Himalaya) and Hindu Kush. For Nyainqêntanglha (named Hengduan Shan and S & E Tibet in the RGI sub-region masks) – one of the most controversial regions – Shean et al. (2020) and Brun et al. (2017) report significantly less negative mass trends (–0.50 ± 0.15 and –0.62 ± 0.23 m w.e. yr⁻¹) than our estimates of –0.97 ± 0.09 m w.e. yr⁻¹, whilst *in situ* measurements (–0.94 m w.e. yr⁻¹ by Yao et al. [2012] based on the Parlung glaciers between 2006 and 2010) and ICESat studies (Kääb et al., 2015; Treichler et al., 2019) find higher negative rates for the survey time period of 2003 to 2008. We also record higher mass losses in Eastern Himalaya / Bhutan, adjacent to the Nyainqêntanglha mountains. The differences in Nyainqêntanglha and Eastern Himalaya between our estimates and the ones of Brun et al. (2017) and Shean et al. (2020) [time

periods 2000-2016 and 2000-2018] fit in with the generally observed acceleration of mass loss in South-East Asia over the past decades (Maurer et al., 2019; Zemp et al., 2019). Some studies suggest the weakening of the Indian summer monsoon as the primary source of increased thinning (Salerno et al., 2015), whilst other studies find no widespread precipitation decrease

285   in monsoonal regimes which could account for all of these changes and attribute the temperature sensitivity of glaciers in monsoon-dominated regions as the main driver (Maurer et al., 2019). In fact, glaciers in Hengduan Shan, Nyainqêntanglha and Eastern Himalaya have been found to exhibit the highest sensitivity towards temperature in the whole HMA region (Sakai and Fujita, 2017).

Contradictory estimates have also been published for the Pamir and Pamir Alay mountains (Hissar Alay), where high (Kääb

290   et al., 2015), moderate (this study), slight mass losses (Brun et al., 2017; Shean et al., 2020), and even mass gains (Gardelle et al., 2013) have been reported. Time series by Ciracì et al. (2020) suggest an acceleration of mass losses within the Pamir-Karakoram region since 2011, which could explain our higher mass loss estimates in comparison to the DEM differencing studies (Brun et al., 2017; Gardelle et al., 2013; Shean et al., 2020). In fact, our time series suggest that the glaciers in Pamir and Hissar Alay were indeed thinning moderately from 2011, with a slowdown from 2016-7 onward.

295   We record less mass gain in Kunlun (+0.01 ± 0.03 m w.e. yr^{-1}; +0.06 ± 0.03 m w.e. yr^{-1} in the Western part of Kunlun) than previous studies – a potential sign for the widely discussed and predicted disappearance of the Karakoram anomaly. However, our time series suggests increased mass gain from 2016 in Western Kunlun, and also mass gain in the Karakoram (Figure 5). At the same time, we also observe decreased thinning rates in Inner Tibet and East Kunlun. These changes could be a short-term trend, however, it displays the limitation of all mentioned studies (including this study) when deriving linear trends in a

300   region like High Mountain Asia with large inter-annual climate variability and associated glacier changes.

We generally find better agreements with Shean et al. (2020) – the study including an additional 2+ years (2017 and 2018) in comparison to Brun et al. (2017), and thus more closely aligned with our time period. This potentially indicates that a large part of the disagreements could be related to inter-annual variability and survey time period.

305   ## 4.2   Gulf of Alaska

4.2.1   Temporal variability

We display temporal variability of surface elevation change for the whole GoA region (Figure 4), the RGI sub-regions (Figure 9, S3) and for different elevation bands within sub-regions (Figure 10). Figure 9 shows negative trends across all the sub-regions. The four coastal sub-regions – Alaska Pena, Western Chugach Mountains, Saint Elias Mountains and Coast Ranges

310   – display a seasonal oscillation, with an annual surface elevation maximum in spring and annual surface elevation minimum in autumn. In contrary, the seasonal cycle of Alaska Range mountains is shifted, with the thickness maximum in winter, which is also somewhat visible in the time series by Luthcke et al. (2008).

A very noticeable feature within the full GoA time series is the steepening (more negative) of inter-annual elevation trends from 2013-4 onwards (Figure 4). We observe a lowering of mean surface elevations almost consistently across all the five sub-
315   regions, but this is most pronounced in the Saint Elias Mountains, the Western Chugach mountains and Coast Ranges. Wouters et al. (2019) and Ciracì et al. (2020) report a similar behaviour around 2014 in time series covering the whole Alaska region. This change correlates with the change from a negative PDO phase to a positive phase in 2014, which resulted in increased temperatures (Wendler et al., 2017). Our findings suggest that the sensitivity of glaciers to the 2014 temperature change increases towards lower elevations (Figure 10). The fact that the strongest impact is observed in the coastal regions is likely
320   due the higher sensitivity of maritime glaciers in Alaska to temperature change (Gregory and Oerlemans, 1998) and the lower elevations within these regions.

4.2.2   Altitudinal distribution

We observe a clear correlation between surface elevation changes and altitude (Figure 11, Table S2), with the highest negative trends at low altitudes in the Saint Elias Mountains and Coast Ranges. In comparison to the study by Berthier et al. (2010),
325   which is based on sequential Digital Elevation Models over the time period from 1962 to 2006, we observe similar elevation changes at the lowest altitudes but less steep gradients in sub-regions along the east coast. This is particularly pronounced in the Saint Elias Mountains, where Berthier et al. (2010) show near-balance at around 1000 metre above sea level, whilst our estimates suggest a surface elevation change of –1.5 m yr^{-1} at the same altitude. These findings indicate a propagation of thinning upstream since 1962 to 2006. In contrary, whilst on the Alaska Peninsula elevation changes have increased at lower
330   altitudes, the limit of the thinning area has stayed the same since the survey time period of Berthier et al. (2010).
In the Western Chugach Mountains, Alaska Range and Alaska Peninsula we observe the effect of debris cover on the altitudinal profile, with a decrease of thinning rates towards the lowest elevations of these sub-regions. This characteristic has been observed, although more pronounced and across all sub-regions, by Berthier et al. (2010) and Arendt et al. (2002).

4.2.3   Comparison of total mass balance with previous work

335   Our total mass budget of –76.3 ± 5.6 Gt yr^{-1} (–0.89 ± 0.07 m w.e. yr^{-1}) agrees with existing estimates, including those using GRACE (−76 ± 4 Gt yr^{-1}, −72.5 ± 8 Gt yr^{-1} and −69 ± 11 Gt yr^{-1} by Sasgen et al., 2012, Ciracì et al., 2020 and Luthcke et al., 2013) and ICESat (−65 ± 12 Gt yr^{-1} by Arendt et al., 2013) as well as a study from airborne altimetry (–75 ± 11 Gt yr^{-1} by Larsen et al., 2015) and a consensus estimate combining glaciological and geodetic observations (–73 ± 17 Gt yr^{-1} / −0.85 ± 0.19 m w.e. yr^{-1} by Zemp et al., 2019) (Figure 8b). Our result is significantly more negative than two GRACE studies, with
340   estimates of −53 ± 14 Gt yr^{-1} (Wouters et al., 2019) and −42 ± 6 Gt yr^{-1} (Jacob et al., 2012). Besides the variations in methodologies and data between these studies, also differences in study area extents, glacier masks and volume to mass conversion factors contribute to the spread of total mass change results. Our estimates correspond to the RGI 1 region (excluding Northern Alaska) to make the results more comparable for future studies. In general, our total mass balance is more

negative than most other studies' findings, reflecting the increased thinning rates we show in the sub-regional time series from

345   2014.

Since there is no prevalent sub-region mask used by more recent studies, we cannot directly compare and validate our results on a sub-regional level. Mass balance or surface elevation change estimates that overlap with our time period are either spatially not resolved (e.g. Gardner et al., 2013; Zemp et al., 2019), presented on a glacier to glacier basis (e.g. Larsen et al., 2015) or GRACE mascon extents (e.g. Luthcke et al., 2008, 2013).

350   Figure 12 displays a comparison with the 1962 to 2006 estimates of Berthier et al. (2010), providing insights into changes of thinning rates since this time period. Our results are consistently more negative, however the general pattern with the lowest changes discovered in Alaska Range and the highest rates taking place in the Coast Ranges is in agreement with Berthier et al. (2010). We see the largest differences along the east coast − particularly in the Saint Elias mountains − which are also the areas where the lowering of mean surface elevations after the PDO event in 2014 has been most pronounced (see Figure 9,

355   S3).

In addition to the comparison with Berthier et al. (2010) we present sub-regional estimates aggregated on the RGI 6.0 second order regions in Table 2 for future reference.

5   Conclusion

We exploit CryoSat-2 interferometric swath processed data from 2010 to 2019, with a total of 33 million elevation

360   observations, to generate new and independent mass balance estimates for two mountain regions, the Gulf of Alaska (GoA) and High Mountain Asia (HMA). We also generate observations at sub-regional level and extract elevation-dependant thinning rates, revealing contrasting mass loss across sub-regions. Finally, we extract monthly time series of elevation change, exploiting CryoSat's high temporal repeat, to reveal seasonal and multiannual variation in rates of glaciers' thinning. We find that between 2010 and 2019, HMA has lost mass at rates of 27.9 ± 2.4 Gt yr^{-1} (0.29 ± 0.03 m w.e. yr^{-1}), and the GoA region

365   has lost mass at rates of 76.3 ± 5.6 Gt yr^{-1} (0.89 ± 0.07 m w.e. yr^{-1}), for a sea-level contribution of 0.048 ± 0.004 mm yr^{-1} and 0.217 ± 0.015 mm yr^{-1} respectively for HMA and the GoA. These estimates are broadly consistent with the range of estimates generated by previous studies and highlight the significant discrepancies that remain in the assessments of mass loss for these two regions.

In HMA we find the most negative surface elevation trends in the Nyainqêntanglha mountains, Hengduan Shan, the East

370   Himalayan range and the Tien Shan and slightly positive/near balance trends in the Kunlun and Karakoram ranges, known as the "Karakoram anomaly". This spatial heterogeneity is known to be influenced by the two main prevailing atmospheric circulation systems in the Himalayas; the Indian summer monsoon and the winter Westerlies. Our monthly time series give insights into the impact of these two systems on glacier dynamics, with the sub-regional accumulation and ablation cycles being influenced by the seasonality of the precipitation. We show sustained multiannual trends across almost all of the

375   subregions until 2015-6, and decreased loss or even mass gain from 2016/2017 onwards.

Negative mass trends are also observed in all of the sub-regions in the GoA region, with the largest mass losses in the Coast Ranges and the Saint Elias Mountains. The GoA time series reveal an increased mass loss from 2014, most pronounced in sub-regions along the south-central and south-east coast (Saint Elias Mountains, Chugach mountains and Coast Ranges) at lower elevations. This mass loss acceleration is linked with the change from a negative to a positive Pacific Decal Oscillation (PDO)
380   in 2014 which resulted in increased temperatures. In general, our time series not only display the sensitivity of glaciers to climatic conditions and changes but also illustrate the limitations of linear models when deriving thickness changes, highlighting the importance of higher temporal resolution to generate robust long-term trends.

This is the first study to demonstrate the ability of interferometric radar altimetry to monitor large-scale change in thickness, mass and sea-level contribution of glaciers across regions of extreme topography. This, along with recent work in the Arctic
385   and Patagonia (Foresta et al., 2016, 2018; Gourmelen et al., 2018; Gray et al., 2015) demonstrates the potential of such a system to monitor trends in ice mass on a global scale and with increased temporal resolution.

Supplement. The supplement related to this article is available online at: [insert_link]

390

Author contributions. NG and LJ designed the study. LJ performed data analyses and prepared the manuscript. NG generated the swath altimetry dataset and contributed to data interpretation. All authors commented on the manuscript.

Competing interests. The authors declare that they have no conflict of interest.

395

Acknowledgements. This work was performed under the European Space Agency's Support to Science Element CryoSat+ Mountain Glacier and we wish to thank the whole project consortium for the interesting discussions and other contributions throughout this project. We are grateful to Jonathan Alford for facilitating the data processing and pipeline and to Alex Horton for processing reference DEMs. We further thank ESA for providing free access to CryoSat-2 data, the Randolph

400 Glacier Inventory (RGI) consortium for providing free access to glacier and debris masks, the German Aerospace Center (DLR) for providing free access to the TanDEM-X DEM and NASA for providing free access to the SRTM DEM.

Financial support. This research has been supported by the ESA project CryoSat+ Mountain Glaciers (contract no. 4000114224/15/I-SBo).

405

6 References

Arendt, A., Luthcke, S., Gardner, A., O'Neel, S., Hill, D., Moholdt, G. and Abdalati, W.: Analysis of a GRACE global mascon solution for Gulf of Alaska glaciers, J. Glaciol., 59(217), 913–924, doi:10.3189/2013JoG12J197, 2013.

410 Arendt, A. A., Echelmeyer, K. A., Harrison, W. D., Lingle, C. S. and Valentine, V. B.: Rapid Wastage of Alaska Glaciers and Their Contribution to Rising Sea Level, Science, 297(5580), 382–386, doi:10.1126/science.1072497, 2002.

Berthier, E., Schiefer, E., Clarke, G. K. C., Menounos, B. and Rémy, F.: Contribution of Alaskan glaciers to sea-level rise derived from satellite imagery, Nat. Geosci., 3(2), 92–95, doi:10.1038/ngeo737, 2010.

Berthier, E., Cabot, V., Vincent, C. and Six, D.: Decadal Region-Wide and Glacier-Wide Mass Balances Derived from Multi-
415 Temporal ASTER Satellite Digital Elevation Models. Validation over the Mont-Blanc Area, Front. Earth Sci., 4, doi:10.3389/feart.2016.00063, 2016.

Bisset, R. R., Dehecq, A., Goldberg, D. N., Huss, M., Bingham, R. G. and Gourmelen, N.: Reversed Surface-Mass-Balance Gradients on Himalayan Debris-Covered Glaciers Inferred from Remote Sensing, Remote Sens., 12(10), 1563, doi:10.3390/rs12101563, 2020.

420 Bojinski, S., Verstraete, M., Peterson, T. C., Richter, C., Simmons, A. and Zemp, M.: The Concept of Essential Climate Variables in Support of Climate Research, Applications, and Policy, Bull. Am. Meteorol. Soc., 95(9), 1431–1443, doi:10.1175/BAMS-D-13-00047.1, 2014.

Bolch, T., Kulkarni, A., Kääb, A., Huggel, C., Paul, F., Cogley, J. G., Frey, H., Kargel, J. S., Fujita, K., Scheel, M., Bajracharya, S. and Stoffel, M.: The State and Fate of Himalayan Glaciers, Science, 336(6079), 310–314, doi:10.1126/science.1215828,
425 2012.

Bolch, T., Shea, J. M., Liu, S., Azam, F. M., Gao, Y., Gruber, S., Immerzeel, W. W., Kulkarni, A., Li, H., Tahir, A. A., Zhang, G. and Zhang, Y.: Status and Change of the Cryosphere in the Extended Hindu Kush Himalaya Region, in The Hindu Kush Himalaya Assessment: Mountains, Climate Change, Sustainability and People, edited by P. Wester, A. Mishra, A. Mukherji, and A. B. Shrestha, pp. 209–255, Springer International Publishing, Cham., 2019.

430 Brun, F., Berthier, E., Wagnon, P., Kääb, A. and Treichler, D.: A spatially resolved estimate of High Mountain Asia glacier mass balances from 2000 to 2016, Nat. Geosci., 10(9), 668–673, doi:10.1038/ngeo2999, 2017.

Ciracì, E., Velicogna, I. and Swenson, S.: Continuity of the Mass Loss of the World's Glaciers and Ice Caps From the GRACE and GRACE Follow-On Missions, Geophys. Res. Lett., 47(9), e2019GL086926, doi:10.1029/2019GL086926, 2020.

Cogley, J. G.: Present and future states of Himalaya and Karakoram glaciers, Ann. Glaciol., 52(59), 69–73,
435 doi:10.3189/172756411799096277, 2011.

Dehecq, A., Gourmelen, N., Shepherd, A., Cullen, R. and Trouvé, E.: Evaluation of CryoSat-2 for height retrieval over the Himalayan range, in CryoSat-2 third user workshop, Dresden, Germany. [online] Available from: https://hal.archives-ouvertes.fr/hal-00973393 (Accessed 25 March 2020), 2013.

Dehecq, A., Gourmelen, N., Gardner, A. S., Brun, F., Goldberg, D., Nienow, P. W., Berthier, E., Vincent, C., Wagnon, P. and
440 Trouvé, E.: Twenty-first century glacier slowdown driven by mass loss in High Mountain Asia, Nat. Geosci., 12(1), 22–27, doi:10.1038/s41561-018-0271-9, 2019.

Farinotti, D., Huss, M., Fürst, J. J., Landmann, J., Machguth, H., Maussion, F. and Pandit, A.: A consensus estimate for the ice thickness distribution of all glaciers on Earth, Nat. Geosci., 12(3), 168–173, doi:10.1038/s41561-019-0300-3, 2019.

445   Fleming, S. W. and Whitfield, P. H.: Spatiotemporal mapping of ENSO and PDO surface meteorological signals in British Columbia, Yukon, and southeast Alaska, Atmosphere-Ocean, 48(2), 122–131, doi:10.3137/AO1107.2010, 2010.

Foresta, L., Gourmelen, N., Pálsson, F., Nienow, P., Björnsson, H. and Shepherd, A.: Surface elevation change and mass balance of Icelandic ice caps derived from swath mode CryoSat-2 altimetry, Geophys. Res. Lett., 43, 12138–12145, doi:10.1002/2016GL071485, 2016.

Foresta, L., Gourmelen, N., Weissgerber, F., Nienow, P., Williams, J. J., Shepherd, A., Drinkwater, M. R. and Plummer, S.:
450   Heterogeneous and rapid ice loss over the Patagonian Ice Fields revealed by CryoSat-2 swath radar altimetry, Remote Sens. Environ., 211, 441–455, doi:10.1016/j.rse.2018.03.041, 2018.

Fujita, K. and Nuimura, T.: Spatially heterogeneous wastage of Himalayan glaciers, Proc. Natl. Acad. Sci., 108(34), 14011–14014, doi:10.1073/pnas.1106242108, 2011.

Gardelle, J., Berthier, E. and Arnaud, Y.: Slight mass gain of Karakoram glaciers in the early twenty-first century, Nat. Geosci.,
455   5(5), 322–325, doi:10.1038/ngeo1450, 2012.

Gardelle, J., Berthier, E., Arnaud, Y. and Kääb, A.: Region-wide glacier mass balances over the Pamir-Karakoram-Himalaya during 1999–2011, The Cryosphere, 7(4), 1263–1286, doi:10.5194/tc-7-1263-2013, 2013.

Gardner, A. S., Moholdt, G., Cogley, J. G., Wouters, B., Arendt, A. A., Wahr, J., Berthier, E., Hock, R., Pfeffer, W. T., Kaser, G., Ligtenberg, S. R. M., Bolch, T., Sharp, M. J., Hagen, J. O., Broeke, M. R. van den and Paul, F.: A Reconciled Estimate of
460   Glacier Contributions to Sea Level Rise: 2003 to 2009, Science, 340(6134), 852–857, doi:10.1126/science.1234532, 2013.

German Aerospace Center (DLR): TanDEM-X - Digital Elevation Model (DEM) - Global, 90m, , doi:10.15489/ju28hc7pui09, 2018.

Gourmelen, N., Escorihuela, M., Shepherd, A., Foresta, L., Muir, A., Garcia-Mondejar, A., Roca, M., Baker, S. and Drinkwater, M. R.: CryoSat-2 swath interferometric altimetry for mapping ice elevation and elevation change, Adv. Space
465   Res., doi:10.1016/j.asr.2017.11.014, 2018.

Gray, L., Burgess, D., Copland, L., Cullen, R., Galin, N., Hawley, R. and Helm, V.: Interferometric swath processing of Cryosat data for glacial ice topography, Cryosphere, 7(6), 1857–1867, doi:10.5194/tc-7-1857-2013, 2013.

Gray, L., Burgess, D., Copland, L., Demuth, M. N., Dunse, T., Langley, K. and Schuler, T. V.: CryoSat-2 delivers monthly and inter-annual surface elevation change for Arctic ice caps, The Cryosphere, 9(5), 1895–1913, doi:10.5194/tc-9-1895-2015,
470   2015.

Gregory, J. M. and Oerlemans, J.: Simulated future sea-level rise due to glacier melt based on regionally and seasonally resolved temperature changes, Nature, 391(6666), 474–476, doi:10.1038/35119, 1998.

Guido, Z., McIntosh, J. C., Papuga, S. A. and Meixner, T.: Seasonal glacial meltwater contributions to surface water in the Bolivian Andes: A case study using environmental tracers, J. Hydrol. Reg. Stud., 8, 260–273, doi:10.1016/j.ejrh.2016.10.002,
475   2016.

Hawley, R. L., Shepherd, A., Cullen, R., Helm, V. and Wingham, D. J.: Ice-sheet elevations from across-track processing of airborne interferometric radar altimetry, Geophys. Res. Lett., 36(22), doi:10.1029/2009GL040416, 2009.

Hodgkins, G. A.: Streamflow changes in Alaska between the cool phase (1947–1976) and the warm phase (1977–2006) of the Pacific Decadal Oscillation: The influence of glaciers, Water Resour. Res., 45(6), doi:10.1029/2008WR007575, 2009.

480   Huss, M.: Density assumptions for converting geodetic glacier volume change to mass change, The Cryosphere, 7(3), 877–887, doi:10.5194/tc-7-877-2013, 2013.

Huss, M. and Hock, R.: Global-scale hydrological response to future glacier mass loss, Nat. Clim. Change, 8(2), 135–140, doi:10.1038/s41558-017-0049-x, 2018.

Immerzeel, W. W., Beek, L. P. H. van and Bierkens, M. F. P.: Climate Change Will Affect the Asian Water Towers, Science, 485   328(5984), 1382–1385, doi:10.1126/science.1183188, 2010.

Jacob, T., Wahr, J., Pfeffer, W. T. and Swenson, S.: Recent contributions of glaciers and ice caps to sea level rise, Nature, 482(7386), 514–518, doi:10.1038/nature10847, 2012.

Kääb, A., Berthier, E., Nuth, C., Gardelle, J. and Arnaud, Y.: Contrasting patterns of early twenty-first-century glacier mass change in the Himalayas, Nature, 488(7412), 495–498, doi:10.1038/nature11324, 2012.

490   Kääb, A., Treichler, D., Nuth, C. and Berthier, E.: Brief Communication: Contending estimates of 2003–2008 glacier mass balance over the Pamir–Karakoram–Himalaya, The Cryosphere, 9(2), 557–564, doi:10.5194/tc-9-557-2015, 2015.

Larsen, C. F., Burgess, E., Arendt, A. A., O'Neel, S., Johnson, A. J. and Kienholz, C.: Surface melt dominates Alaska glacier mass balance, Geophys. Res. Lett., 42(14), 5902–5908, doi:10.1002/2015GL064349, 2015.

Le Bris, R., Paul, F., Frey, H. and Bolch, T.: A new satellite-derived glacier inventory for western Alaska, Ann. Glaciol., 495   52(59), 135–143, doi:10.3189/172756411799096303, 2011.

Li, Z., Fang, H., Tian, L., Dai, Y. and Zong, J.: Changes in the glacier extent and surface elevation in Xiongcaigangri region, Southern Karakoram Mountains, China, Quat. Int., 371, doi:10.1016/j.quaint.2014.12.004, 2015.

Luthcke, S. B., Arendt, A. A., Rowlands, D. D., McCarthy, J. J. and Larsen, C. F.: Recent glacier mass changes in the Gulf of Alaska region from GRACE mascon solutions, J. Glaciol., 54(188), 767–777, doi:10.3189/002214308787779933, 2008.

500   Luthcke, S. B., Sabaka, T. J., Loomis, B. D., Arendt, A. A., McCarthy, J. J. and Camp, J.: Antarctica, Greenland and Gulf of Alaska land-ice evolution from an iterated GRACE global mascon solution, J. Glaciol., 59(216), 613–631, doi:10.3189/2013JoG12J147, 2013.

Maurer, J. M., Schaefer, J. M., Rupper, S. and Corley, A.: Acceleration of ice loss across the Himalayas over the past 40 years, Sci. Adv., 5(6), eaav7266, doi:10.1126/sciadv.aav7266, 2019.

505   McMillan, M., Shepherd, A., Sundal, A., Briggs, K., Muir, A., Ridout, A., Hogg, A. and Wingham, D.: Increased ice losses from Antarctica detected by CryoSat-2, Geophys. Res. Lett., 41(11), 3899–3905, doi:10.1002/2014GL060111, 2014a.

McMillan, M., Shepherd, A., Gourmelen, N., Dehecq, A., Leeson, A., Ridout, A., Flament, T., Hogg, A., Gilbert, L., Benham, T., Broeke, M. van den, Dowdeswell, J. A., Fettweis, X., Noël, B. and Strozzi, T.: Rapid dynamic activation of a marine-based Arctic ice cap, Geophys. Res. Lett., 41(24), 8902–8909, doi:10.1002/2014GL062255, 2014b.

510   Moholdt, G., Hagen, J. O., Eiken, T. and Schuler, T. V.: Geometric changes and mass balance of the Austfonna ice cap, Svalbard, The Cryosphere, 4(1), 21–34, doi:10.5194/tc-4-21-2010, 2010a.

Moholdt, G., Nuth, C., Hagen, J. O. and Kohler, J.: Recent elevation changes of Svalbard glaciers derived from repeat track ICESat altimetry, Remote Sens. Environ., 114(11), 2756–2767, doi:10.1016/j.rse.2010.06.008, 2010b.

Neckel, N., Kropáček, J., Bolch, T. and Hochschild, V.: Glacier mass changes on the Tibetan Plateau 2003–2009 derived from ICESat laser altimetry measurements, Environ. Res. Lett., 9(1), 014009, doi:10.1088/1748-9326/9/1/014009, 2014.

Nilsson, J., Sandberg Sørensen, L., Barletta, V. R. and Forsberg, R.: Mass changes in Arctic ice caps and glaciers: implications of regionalizing elevation changes, The Cryosphere, 9(1), 139–150, doi:10.5194/tc-9-139-2015, 2015.

Papineau, J. M.: Wintertime temperature anomalies in Alaska correlated with ENSO and PDO, Int. J. Climatol., 21(13), 1577–1592, doi:10.1002/joc.686, 2001.

Pohl, E., Gloaguen, R. and Seiler, R.: Remote Sensing-Based Assessment of the Variability of Winter and Summer Precipitation in the Pamirs and Their Effects on Hydrology and Hazards Using Harmonic Time Series Analysis, Remote Sens., 7(8), 9727–9752, doi:10.3390/rs70809727, 2015.

Pritchard, H. D.: Asia's shrinking glaciers protect large populations from drought stress, Nature, 569(7758), 649–654, doi:10.1038/s41586-019-1240-1, 2019.

Ragettli, S., Immerzeel, W. W. and Pellicciotti, F.: Contrasting climate change impact on river flows from high-altitude catchments in the Himalayan and Andes Mountains, Proc. Natl. Acad. Sci. U. S. A., 113(33), 9222–9227, doi:10.1073/pnas.1606526113, 2016.

RGI Consortium: Randolph Glacier Inventory – A Dataset of Global Glacier Outlines: Version 6.0, Technical Report, Global Land Ice Measurements from Space, Digit. Media, doi:10.7265/N5-RGI-60, 2017.

Sakai, A. and Fujita, K.: Contrasting glacier responses to recent climate change in high-mountain Asia, Sci. Rep., 7(1), 13717, doi:10.1038/s41598-017-14256-5, 2017.

Salerno, F., Guyennon, N., Thakuri, S., Viviano, G., Romano, E., Vuillermoz, E., Cristofanelli, P., Stocchi, P., Agrillo, G., Ma, Y. and Tartari, G.: Weak precipitation, warm winters and springs impact glaciers of south slopes of Mt. Everest (central Himalaya) in the last 2 decades (1994–2013), The Cryosphere, 9(3), 1229–1247, 2015.

Sasgen, I., Klemann, V. and Martinec, Z.: Towards the inversion of GRACE gravity fields for present-day ice-mass changes and glacial-isostatic adjustment in North America and Greenland, J. Geodyn., 59–60, 49–63, doi:10.1016/j.jog.2012.03.004, 2012.

Scagliola, M., Fornari, M., Bouffard, J. and Parrinello, T.: The CryoSat interferometer: End-to-end calibration and achievable performance, Adv. Space Res., 62(6), 1516–1525, doi:10.1016/j.asr.2017.09.024, 2018.

Shean, D. E., Bhushan, S., Montesano, P., Rounce, D. R., Arendt, A. and Osmanoglu, B.: A Systematic, Regional Assessment of High Mountain Asia Glacier Mass Balance, Front. Earth Sci., 7, doi:10.3389/feart.2019.00363, 2020.

Shepherd, A., Ivins, E., Rignot, E., Smith, B., van den Broeke, M., Velicogna, I., Whitehouse, P., Briggs, K., Joughin, I., Krinner, G., Nowicki, S., Payne, T., Scambos, T., Schlegel, N., A, G., Agosta, C., Ahlstrøm, A., Babonis, G., Barletta, V. R., Bjørk, A. A., Blazquez, A., Bonin, J., Colgan, W., Csatho, B., Cullather, R., Engdahl, M. E., Felikson, D., Fettweis, X., Forsberg, R., Hogg, A. E., Gallee, H., Gardner, A., Gilbert, L., Gourmelen, N., Groh, A., Gunter, B., Hanna, E., Harig, C., Helm, V., Horvath, A., Horwath, M., Khan, S., Kjeldsen, K. K., Konrad, H., Langen, P. L., Lecavalier, B., Loomis, B., Luthcke, S., McMillan, M., Melini, D., Mernild, S., Mohajerani, Y., Moore, P., Mottram, R., Mouginot, J., Moyano, G., Muir, A., Nagler, T., Nield, G., Nilsson, J., Noël, B., Otosaka, I., Pattle, M. E., Peltier, W. R., Pie, N., Rietbroek, R., Rott, H.,

Sandberg Sørensen, L., Sasgen, I., Save, H., Scheuchl, B., Schrama, E., Schröder, L., Seo, K.-W., Simonsen, S. B., Slater, T.,
550   Spada, G., Sutterley, T., Talpe, M., Tarasov, L., van de Berg, W. J., van der Wal, W., van Wessem, M., Vishwakarma, B. D.,
Wiese, D., Wilton, D., Wagner, T., Wouters, B., Wuite, J. and The IMBIE Team: Mass balance of the Greenland Ice Sheet
from 1992 to 2018, Nature, 579(7798), 233–239, doi:10.1038/s41586-019-1855-2, 2020.

Trantow, T. and Herzfeld, U. C.: Spatiotemporal mapping of a large mountain glacier from CryoSat-2 altimeter data: surface
elevation and elevation change of Bering Glacier during surge (2011–2014), Int. J. Remote Sens., 37(13), 2962–2989,
555   doi:10.1080/01431161.2016.1187318, 2016.

Treichler, D., Kääb, A., Salzmann, N. and Xu, C.-Y.: Recent glacier and lake changes in High Mountain Asia and their relation
to precipitation changes, The Cryosphere, 13(11), 2977–3005, doi:10.5194/tc-13-2977-2019, 2019.

Wagnon, P., Vincent, C., Arnaud, Y., Berthier, E., Vuillermoz, E., Gruber, S., Ménégoz, M., Gilbert, A., Dumont, M., Shea,
J. M., Stumm, D. and Pokhrel, B. K.: Seasonal and annual mass balances of Mera and Pokalde glaciers (Nepal Himalaya) since
560   2007, The Cryosphere, 7(6), 1769–1786, doi:10.5194/tc-7-1769-2013, 2013.

Wendler, G., Gordon, T. and Stuefer, M.: On the Precipitation and Precipitation Change in Alaska, Atmosphere, 8(12), 253,
doi:10.3390/atmos8120253, 2017.

Wouters, B., Gardner, A. S. and Moholdt, G.: Global Glacier Mass Loss During the GRACE Satellite Mission (2002-2016),
Front. Earth Sci., 7, doi:10.3389/feart.2019.00096, 2019.

565   Yao, T., Thompson, L., Yang, W., Yu, W., Gao, Y., Guo, X., Yang, X., Duan, K., Zhao, H., Xu, B., Pu, J., Lu, A., Xiang, Y.,
Kattel, D. B. and Joswiak, D.: Different glacier status with atmospheric circulations in Tibetan Plateau and surroundings, Nat.
Clim. Change, 2(9), 663–667, doi:10.1038/nclimate1580, 2012.

Zemp, M., Huss, M., Thibert, E., Eckert, N., McNabb, R., Huber, J., Barandun, M., Machguth, H., Nussbaumer, S. U., Gärtner-
Roer, I., Thomson, L., Paul, F., Maussion, F., Kutuzov, S. and Cogley, J. G.: Global glacier mass changes and their
570   contributions to sea-level rise from 1961 to 2016, Nature, 568(7752), 382–386, doi:10.1038/s41586-019-1071-0, 2019.

Zheng, W., Pritchard, M. E., Willis, M. J., Tepes, P., Gourmelen, N., Benham, T. J. and Dowdeswell, J. A.: Accelerating
glacier mass loss on Franz Josef Land, Russian Arctic, Remote Sens. Environ., 211, 357–375, doi:10.1016/j.rse.2018.04.004,
2018.

575
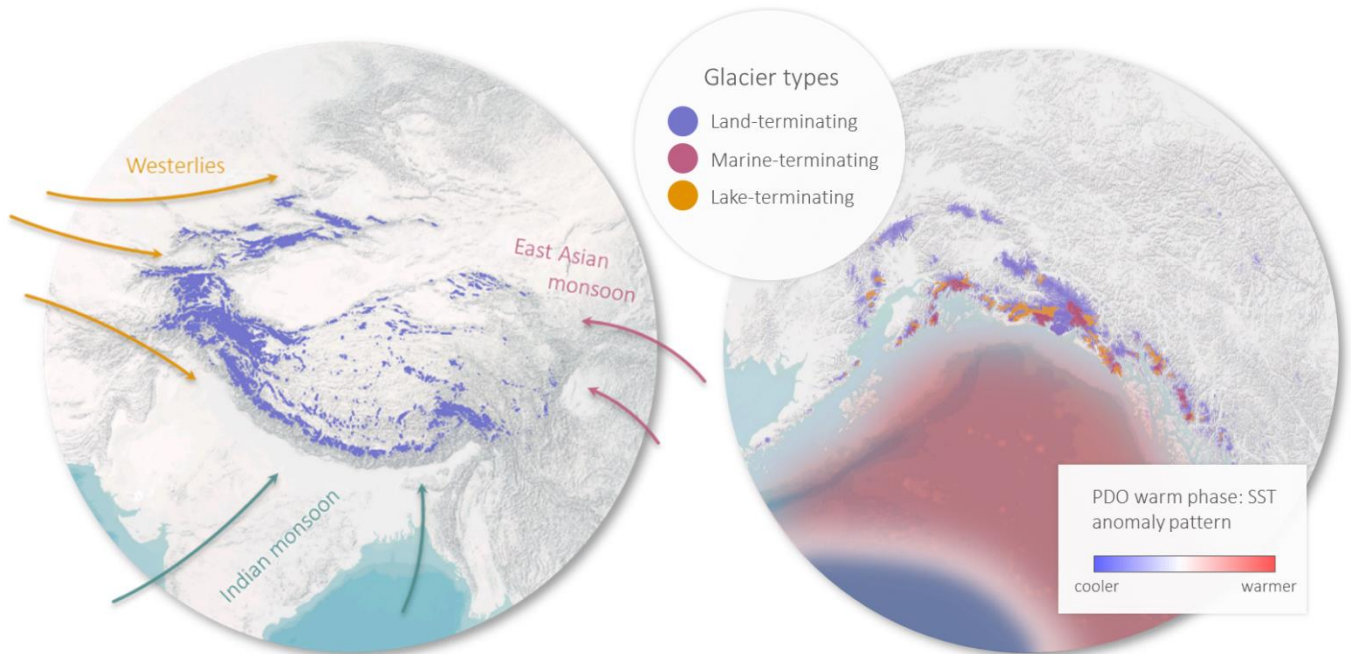
Figure 1: The two study areas. *Left*: **High Mountain Asia (HMA) glaciers with arrows showing the main atmospheric circulation**
580 **systems.** *Right:* **The Gulf of Alaska (GoA) glaciers coloured by glacier type (land-terminating, marine-terminating and lake-terminating). The Sea Surface Temperature (SST) anomaly of the Pacific Decal Oscillation warm/positive phase is displayed in blue-white-red shading.**
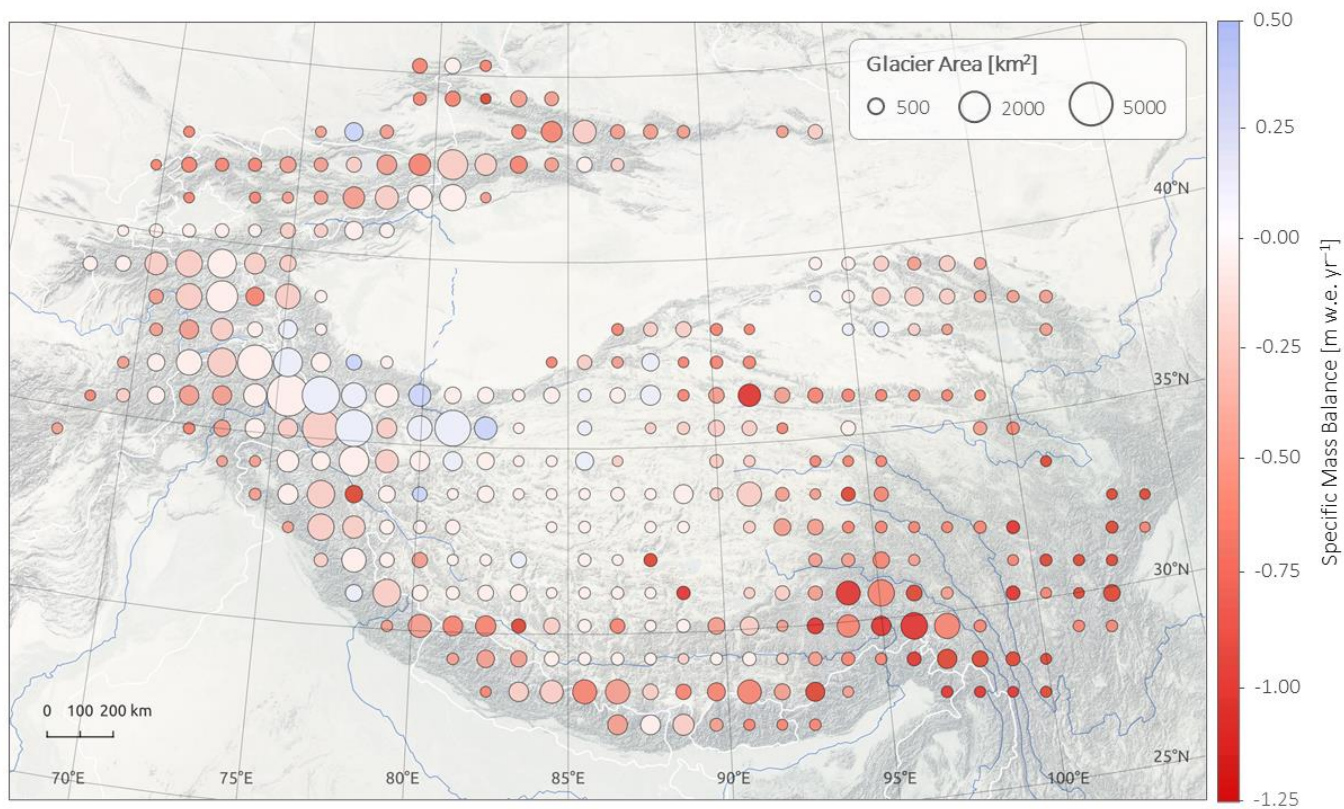
Figure 2: Specific glacier mass balance (m w.e. yr⁻¹) in High Mountain Asia (HMA) for the period of 2010 to 2019 on a 100 x 100 km grid. The size of the circles is scaled by the total glacierised area within a 100 x 100 km bin.
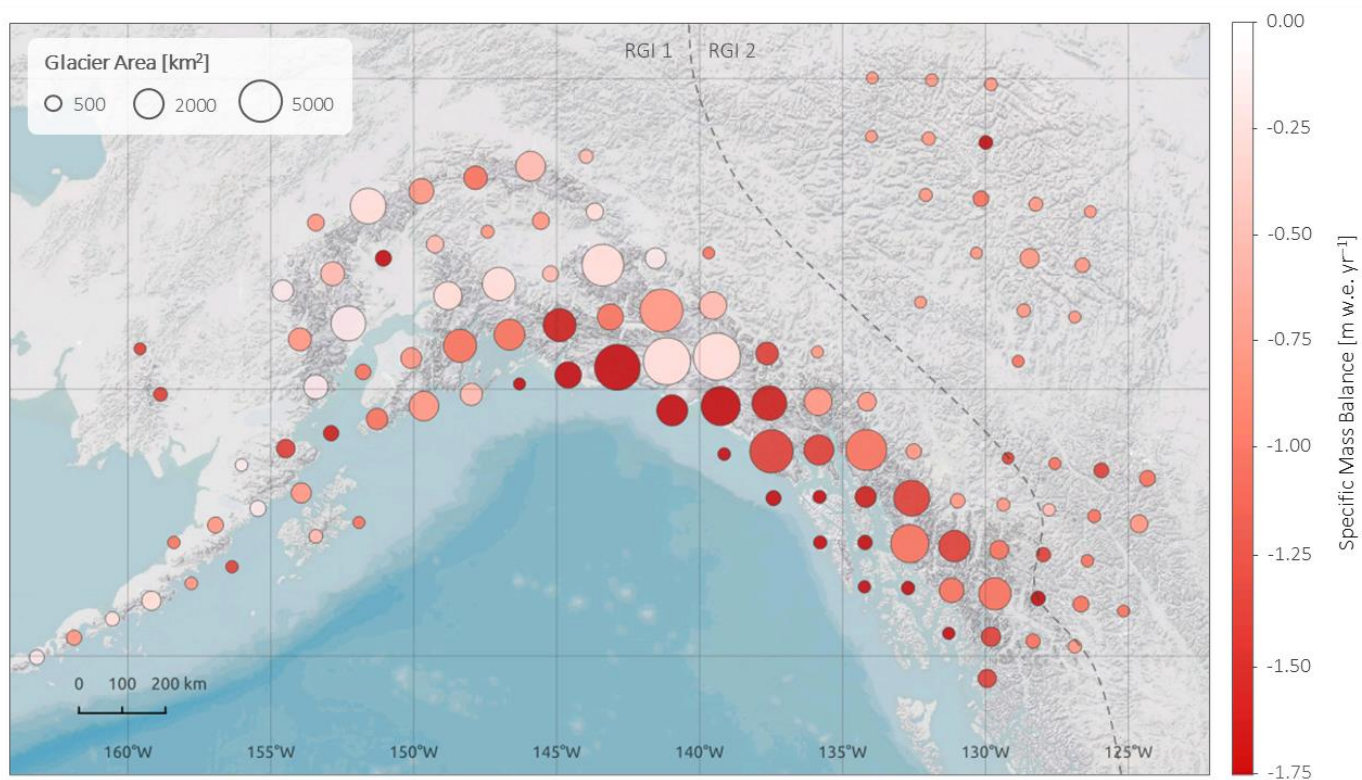
Figure 3: Specific glacier mass balance (m w.e. yr⁻¹) in the Gulf of Alaska (GoA) for the period of 2010 to 2019 on a 100 x 100 km grid. The size of the circles is scaled by the total glacierised area within a cell. Note that our total mass change estimate of –76.3 ± 5.6 Gt yr⁻¹ (–0.89 ± 0.07 m w.e. yr⁻¹) only include glaciers from the RGI region 1 (Alaska). Including also the Northern Rocky Mountains and the Mackenzie and Selwyn mountains we retrieve a mass change of –77.7 ± 5.7 Gt yr⁻¹.
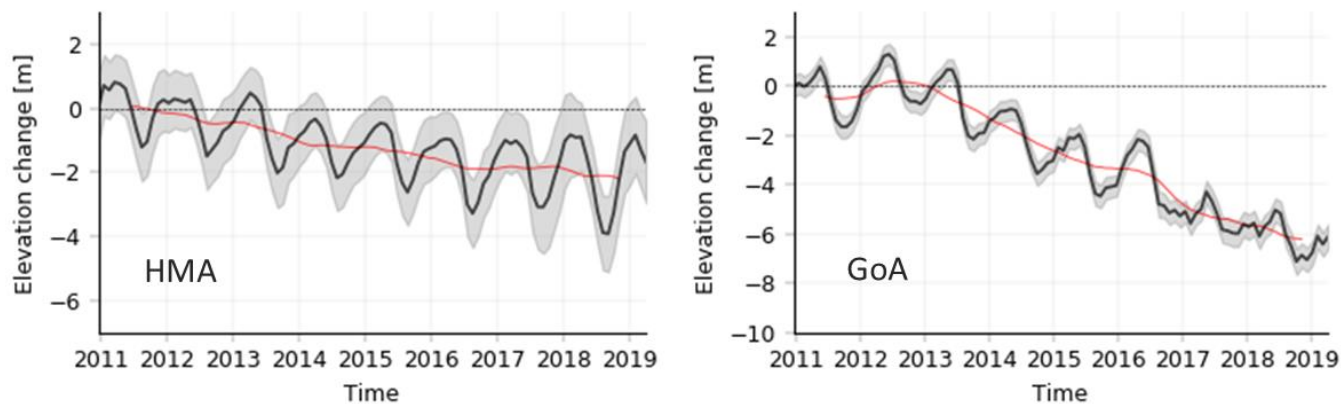
Figure 4: Monthly surface elevation change time series for High Mountain Asia (*left*) and the Gulf of Alaska (GoA) region (*right*). The grey lines display the elevation change time series with the uncertainty envelope. The red line displays a 12-month moving average.
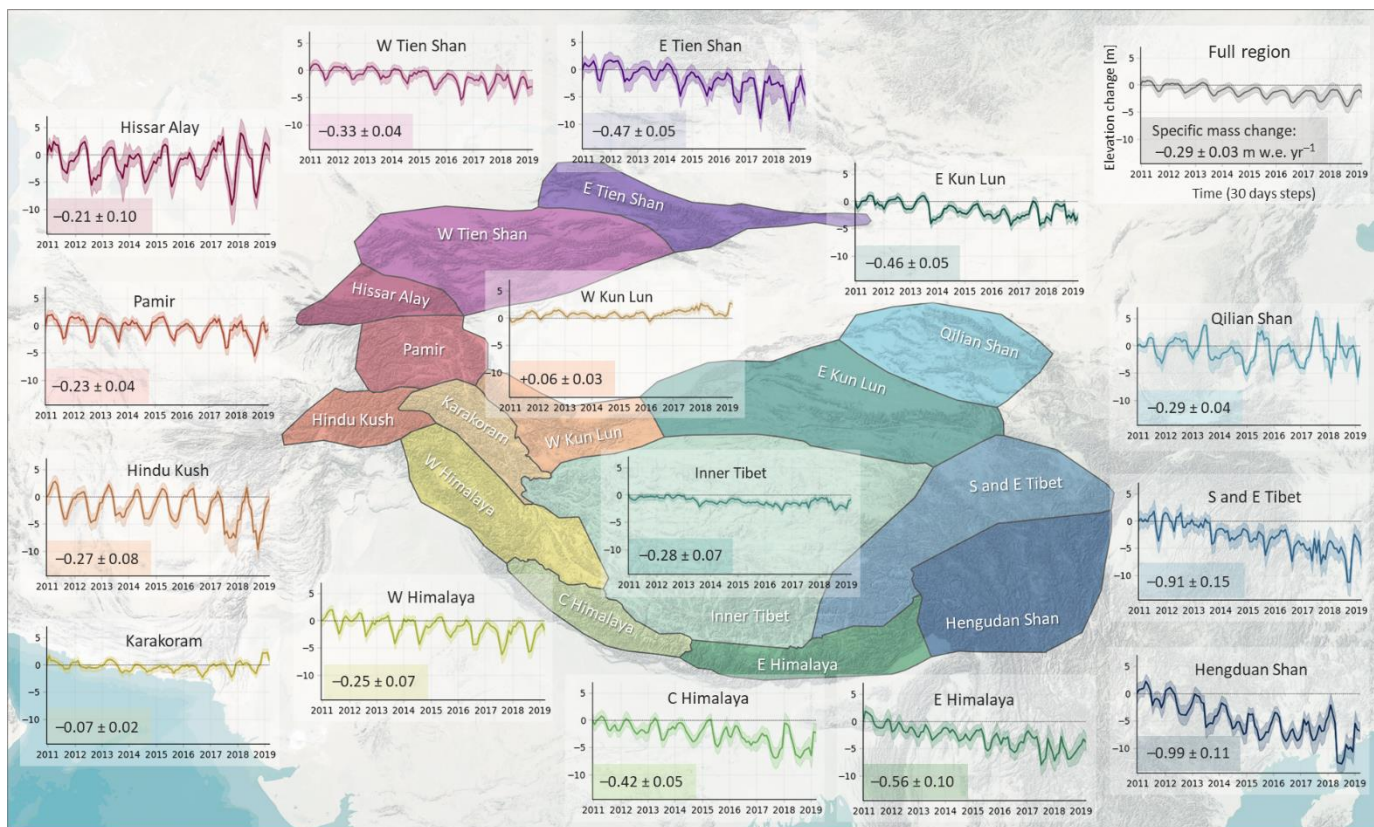
Figure 5: High Mountain Asia (HMA) 30-day elevation change time series in the RGI 6.0 second order regions. The coloured line displays the time series with the uncertainty envelope (*y-axis*: elevation change [m], *x-axis*: time [30-days steps]). The numbers describe the specific mass change with uncertainties in m w.e. yr^{-1}.
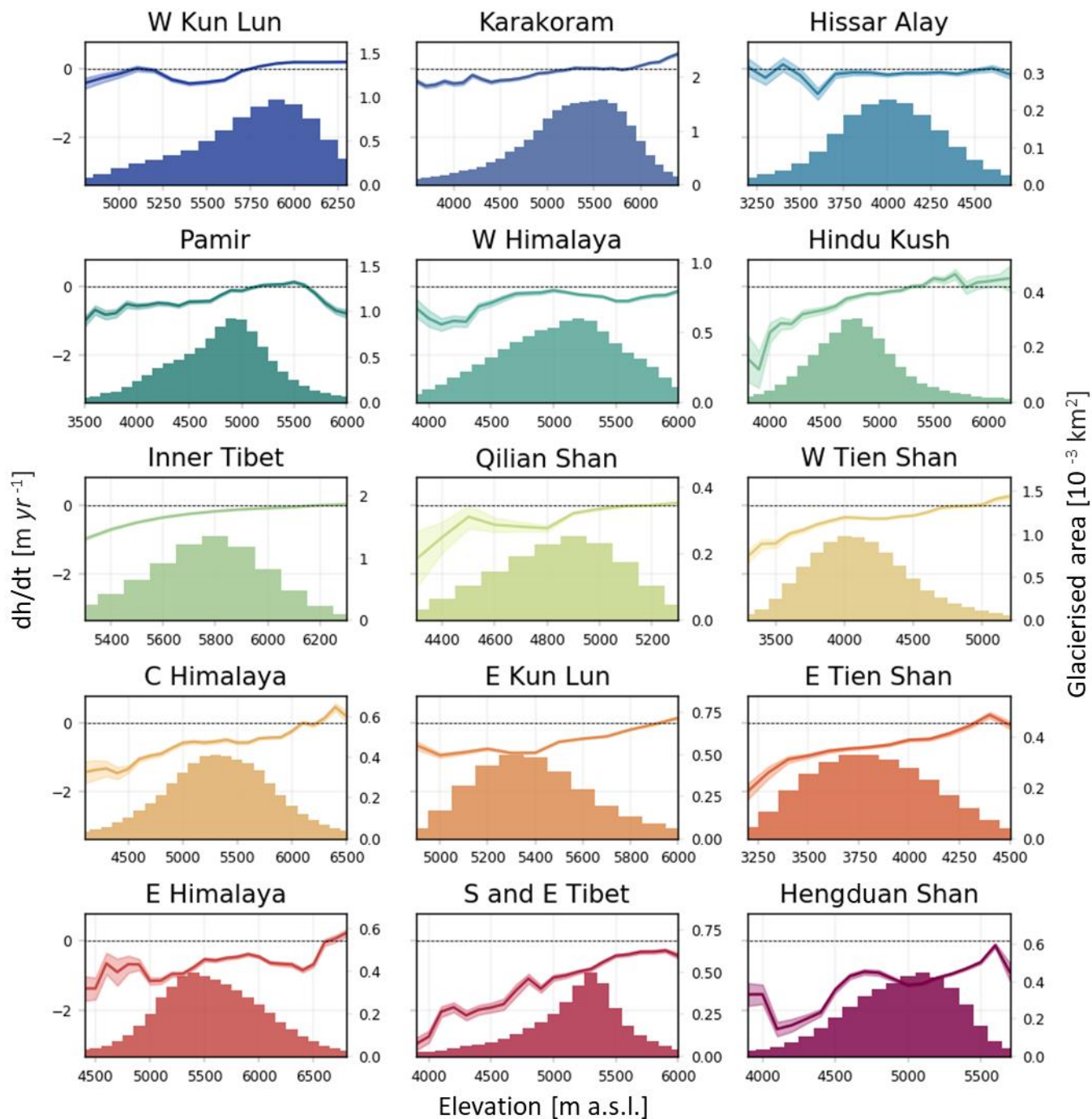
Figure 6: Altitudinal distribution of elevation changes and glacier hypsometry functions in High Mountain Asia (HMA) in RGI 6.0 sub-regions between 2010 and 2019. The lines show elevation change rates with uncertainty envelopes plotted against 100 m elevation bands (*left y-axis*). The bars display the glacier hypsometry (*right y-axis*).

605
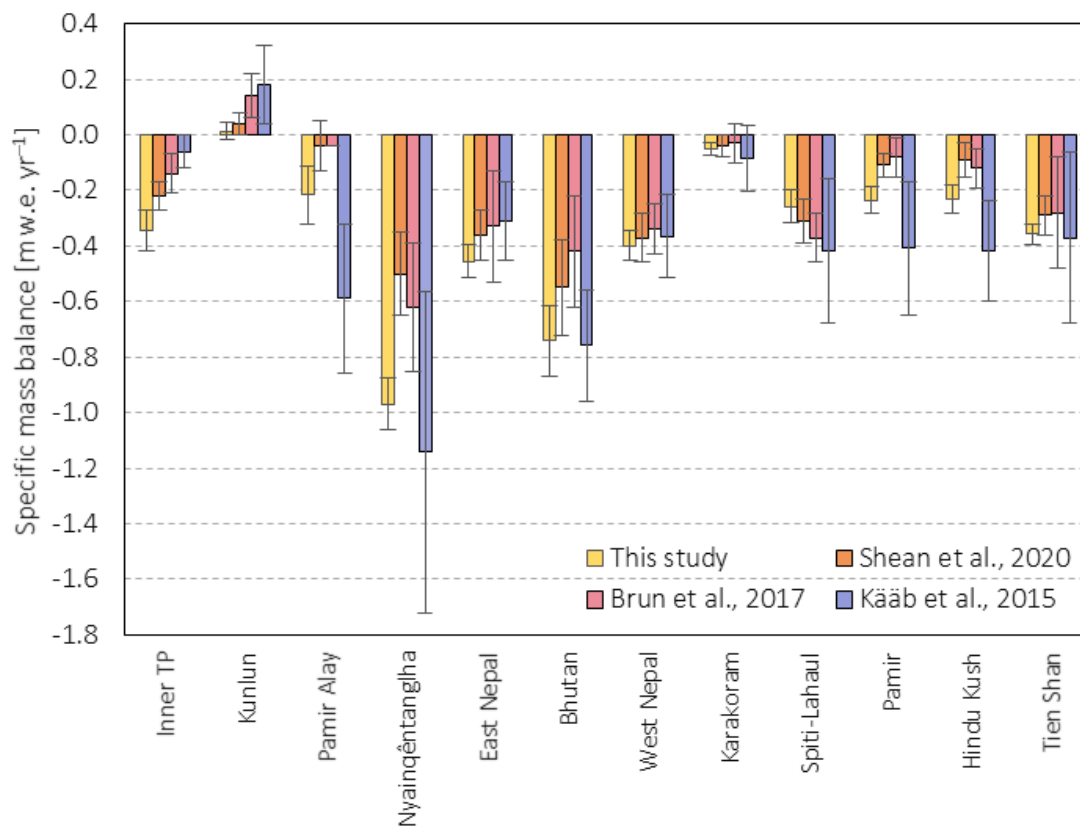
610

Figure 7: High Mountain Asia (HMA) specific mass balance trends on a sub-regional level (using the sub-regions of Brun et al. [2017]) in comparison with DEM differencing and ICESat studies. It is important to note that Shean et al. (2020) cover the time period of 2000 to 2018, Brun et al. (2017) cover the time period of 2000 to 2016 and Kääb et al. (2015) cover the time period 2003 to 2008, whilst this study covers the time period of 2010 to 2019. We have complemented the data from Kääb et al. (2015) with ICESat
615 **data from Brun et al. (2017) for the sub-regions Kunlun, Inner TP, Tien Shan and Pamir Alay, which extended the estimates of Kääb et al. (2015) using the same method.**
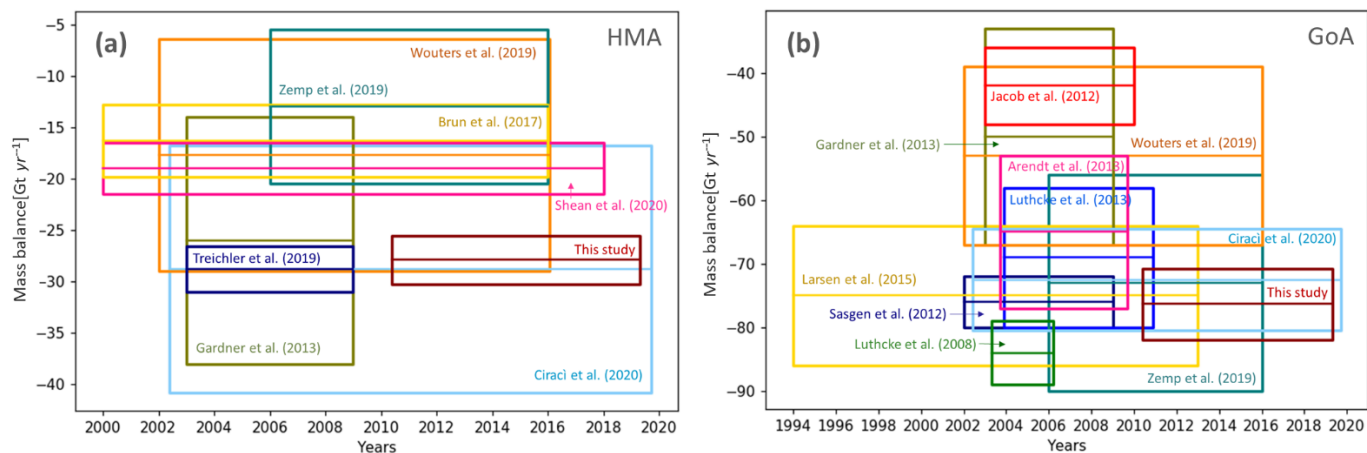
Figure 8: Estimates of mass balance [Gt yr⁻¹] as published in different studies for High Mountain Asia (*left*) and Alaska (*right*).

620
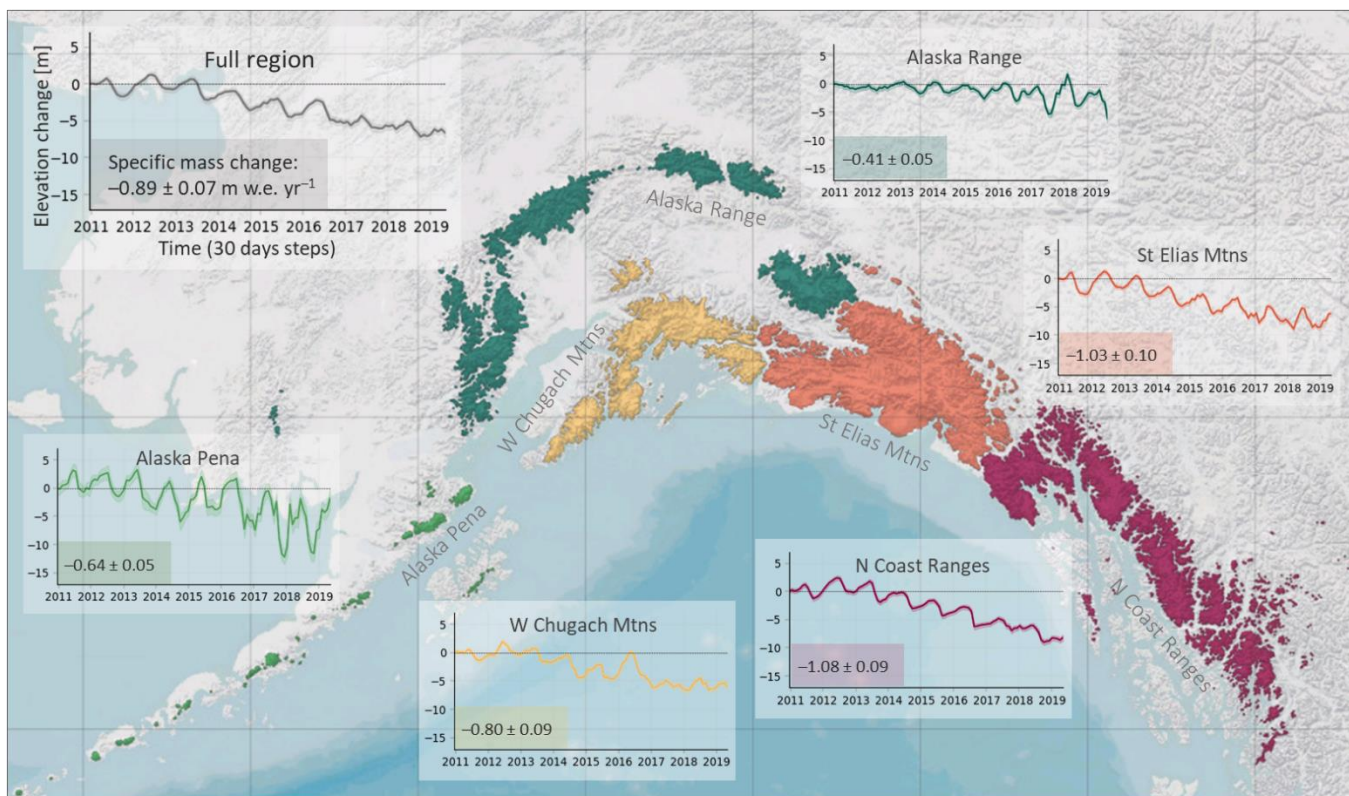
Figure 9: Gulf of Alaska (GoA) monthly elevation change time series on sub-regional level. The coloured lines display the time series with the uncertainty envelope (*y-axis*: elevation change [m], *x-axis*: time [30-days steps]). The numbers describe the specific mass change with uncertainties in m w.e. yr⁻¹.

625
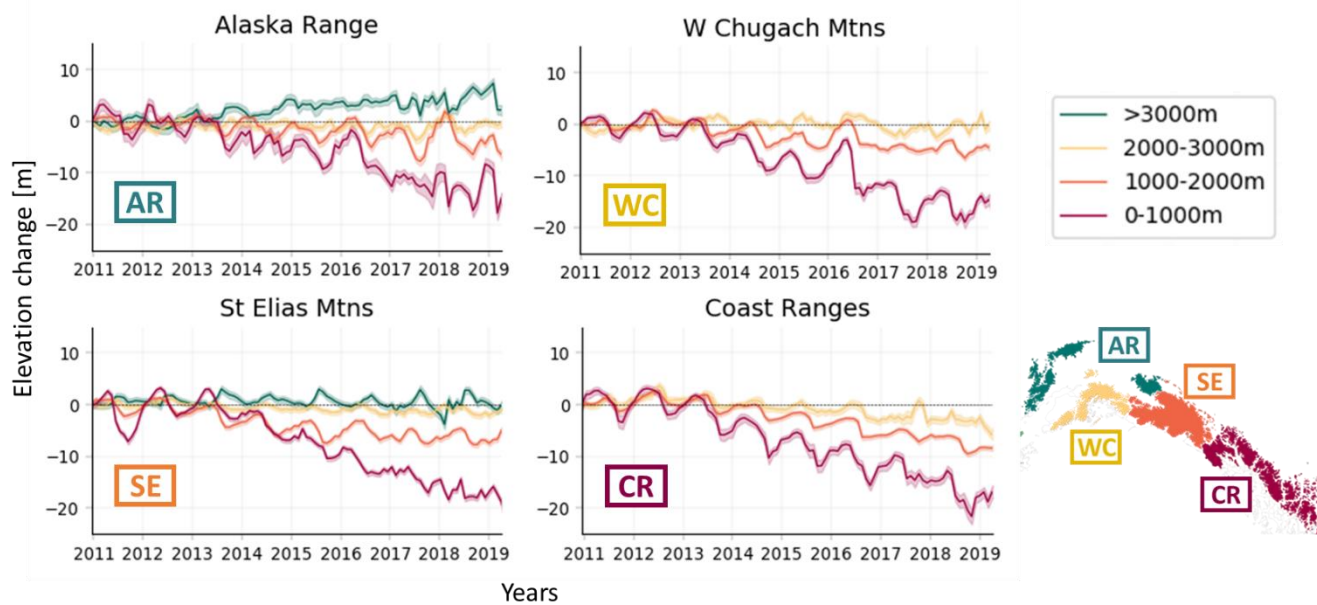
Figure 10: Gulf of Alaska (GoA) monthly surface elevation change time series with uncertainty envelopes at different elevation bands aggregated on the RGI 6.0 second order regions. The different colours represent the elevation bands (>3000 m, 2000-3000 m, 1000-2000 m, 0-2000 m).
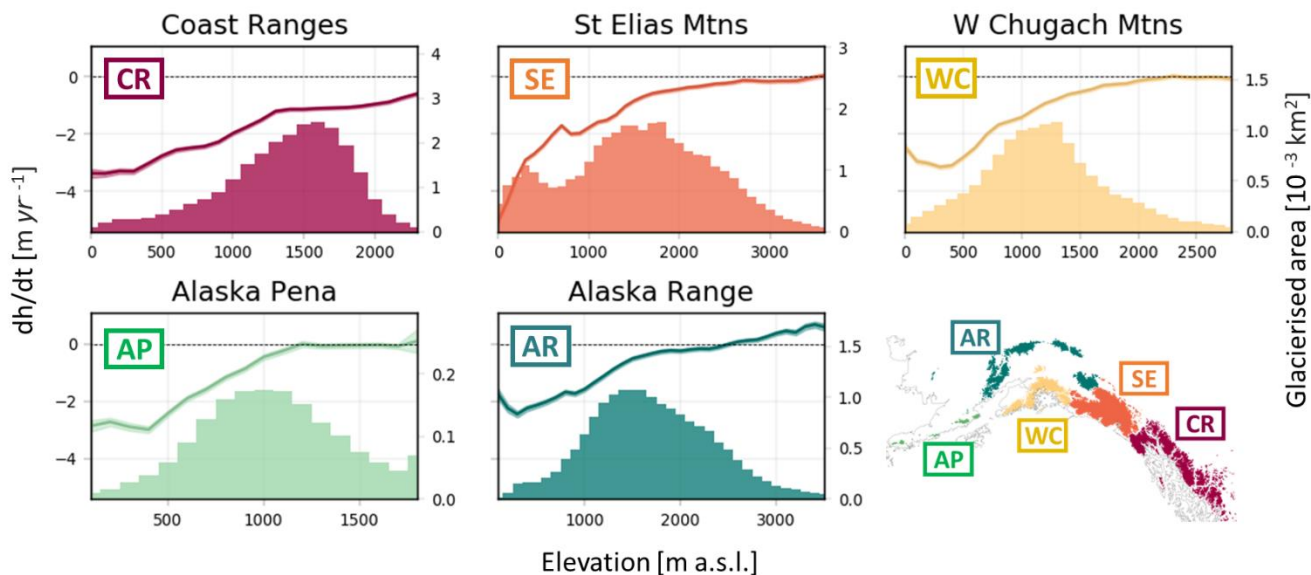
635

Figure 11: Altitudinal distribution of elevation changes and glacier hypsometry functions in the Gulf of Alaska (GoA) in RGI 6.0 sub-regions between 2010 and 2019. The lines show elevation change rates with uncertainty envelopes plotted against 100 metre elevation bands (*left y-axis*). The bars display the glacier hypsometry (*right y-axis*).
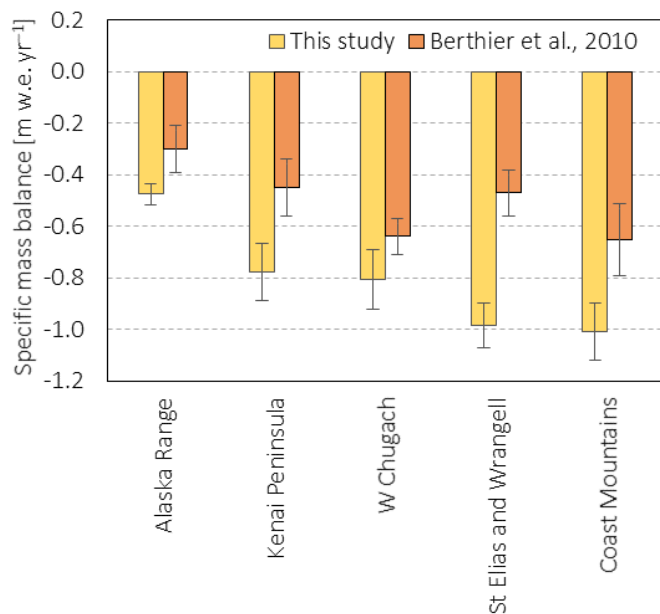
640

Figure 12: Gulf of Alaska (GoA) specific mass balance trends, aggregated on the sub-regions by Berthier et al. (2010). The figure compares our results (2010 to 2019) to the estimates of Berthier et al. (2010), covering the time period 1962 to 2006.

645

	Glacier area [km²]	Specific mass change [m w.e. yr⁻¹]	Mass change [Gt yr⁻¹]
W Tien Shan	9531	−0.33 ± 0.04	−3.09 ± 0.39
E Tien Shan	2854	−0.47 ± 0.05	−1.34 ± 0.14
C Himalaya	5447	−0.42 ± 0.05	−2.30 ± 0.28
W Kun Lun	8153	+0.06 ± 0.03	+0.51 ± 0.26
E Himalaya	4904	−0.56 ± 0.10	−2.76 ± 0.47
E Kun Lun	3251	−0.46 ± 0.05	−1.48 ± 0.17
Hengduan Shan	4383	−0.99 ± 0.11	−4.32 ± 0.47
Qilian Shan	1637	−0.29 ± 0.04	−0.47 ± 0.06
Inner Tibet	7923	−0.28 ± 0.07	−2.22 ± 0.53
S and E Tibet	3873	−0.91 ± 0.15	−3.51 ± 0.57
Hindu Kush	2938	−0.27 ± 0.08	−0.78 ± 0.22
Karakoram	22862	−0.07 ± 0.02	−1.49 ± 0.50
W Himalaya	7768	−0.25 ± 0.07	−1.94 ± 0.53
Hissar Alay	1846	−0.21 ± 0.10	−0.39 ± 0.19
Pamir	10234	−0.23 ± 0.04	−2.33 ± 0.44
Total	97604		

Table 1: High Mountain Asia (HMA) mass balance trends from 2010 to 2019, aggregated on the Randolph Glacier Inventory (RGI 6.0) sub- regions.

	Glacier area [km²]	Specific mass change [m w.e. yr⁻¹]	Mass change [Gt yr⁻¹]
Alaska Range (Wrangell/Kilbuck)	16278	−0.41 ± 0.05	−6.6 ± 0.9
Alaska Pena (Aleutians)	1912	−0.64 ± 0.05	−1.2 ± 0.1
West Chugach Mountains (Talkeetna)	12052	−0.80 ± 0.09	−9.6 ± 1.0
Saint Elias Mountains	33174	−1.03 ± 0.10	−34.1 ± 3.4
Northern Coast Ranges	22963	−1.08 ± 0.09	−24.8 ± 2.1
Total	86379		

650

Table 2: Gulf of Alaska (GoA) mass balance trends from 2010 to 2019, aggregated on the Randolph Glacier Inventory (RGI 6.0) sub- regions.